

# Interior Pointwise Feedback Control and Optimization of Euler Equations for Flow Separation in Stator Cascades by Air Injection

Nhan T. Nguyen\*

*NASA Ames Research Center, Moffett Field, CA 94035*

Michelle M. Bright<sup>†</sup>

Dennis Culley<sup>‡</sup>

*NASA Glenn Research Center, Cleveland, OH 44135*

**This paper presents an adaptive flow control approach for controlling flow separation in a stator cascade within a low-speed axial-flow compressor using an air injection technique. Flow separation usually manifests itself as an increase in a total pressure loss across a blade row. A 1-D unsteady flow model based on the Euler equations incorporating a pressure loss parameter is used to design a feedback control of the total pressure at the outlet. The air injection control is formulated as a pointwise control in the interior region of the solution domain of the Euler equations. The feedback adaptive control strategy relies on a recursive least-square parameter estimation to estimate the effectiveness of air injection. A nonlinear trajectory optimization is developed in order to determine an optimal air injection gain schedule. A gradient-based computational procedure based on a wave-splitting finite-difference method is implemented for the optimization method. Disturbances due to variations in the inlet flow condition at the stator blade row are minimized by a quasi-steady state error-correction feedback optimal control in order to maintain a desired air injection value. The nonlinear optimization and quasi-steady state feedback optimal control are based on a recent adjoint method for the Euler equations. A numerical simulation demonstrates the effectiveness of the proposed flow control strategy.**

## I. Introduction

An aircraft gas turbine engine comprises several major aero-mechanical components including compressors, combustors, and turbines. Within a compressor stage, stator and rotor cascades provide alternate flow passages through which a diffusion process takes place that results in an increase in the static pressure. Under critical operating conditions such as those during takeoff and landing, mass flow deficit or inlet distortion may result. As a consequence, the incidence angle on the blade row may increase substantially beyond an acceptable limit, thus causing stall and flow separation. Current research in flow control in gas turbine engines addresses the needs for improving the design and operation of compressors by flow control augmentation methods. The benefits of flow control technologies could one day lead to new aircraft gas turbine engines that would be more efficient to operate by lowering the fuel consumption, or more environmentally friendly by reducing harmful NOx emissions.<sup>1</sup>

Compressor flow control methods have been investigated by many researchers and there exists a large body of knowledge pertaining to this area of research.<sup>2-4</sup> Recently, a fluid injection flow control concept has been developed at NASA Glenn Research Center for flow separation control in a stator cascade.<sup>5</sup> Highly specialized flow control vanes are fabricated to incorporate a series of air injection slots on the suction surface as shown in Fig. 1.

---

\*Computer Scientist, Intelligent Systems Division, Mail Stop 269-1

<sup>†</sup>Research Engineer, Control and Dynamics Technology Branch, Mail Stop 77-1

<sup>‡</sup>Research Engineer, Control and Dynamics Technology Branch, Mail Stop 77-1

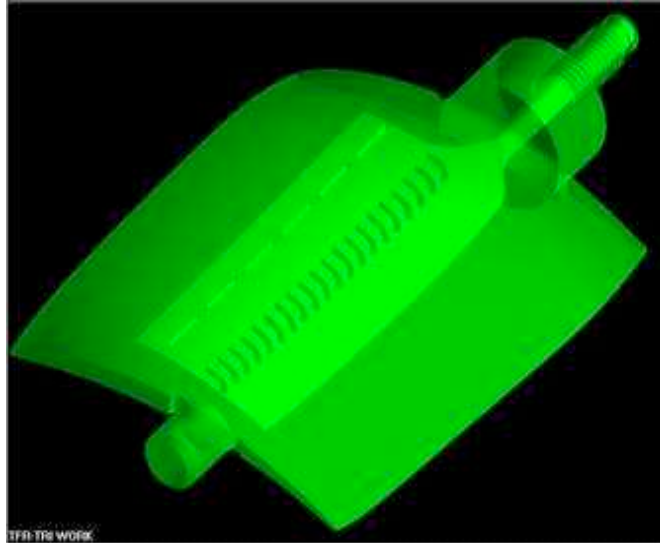


Fig. 1 - Flow Control Stator Vane

The air injection coverage is from approximately 10% to 90% of span and is constrained by the vane cavity design. The flow control vanes produce steady injection or unsteady injection when coupled with an external flow modulating valve. The optimal air injection location is on the suction surface at 35% of chord as determined in a wind tunnel study performed by the Illinois Institute of Technology.<sup>5</sup> In all vane configurations, the injection angle is pitched at 30° relative to the vane upper surface to impart a streamwise momentum to the flow. The working principle of the air injection flow control is based on the well-known boundary layer physics which shows that the boundary layer growth can usually be attenuated by a high momentum small-scale flow, which helps energize the low momentum air accumulated near the blade suction surface by promoting fluid momentum exchange. Experimental testing in the Low Speed Axial-Flow Compressor (LSAC) test facility at NASA Glenn Research Center has demonstrated that this flow control method is effective in reducing a flow blockage caused by a boundary layer growth formed within a stator cascade.<sup>5</sup> The current flow control concept is an open-loop implementation without any feedback. This study will address the feedback design for this flow control concept.



Fig. 2 - NASA Glenn Low Speed Axial-Flow Compressor (LSAC) Test Facility

Fig. 2 shows the LSAC test facility. The LSAC compressor is driven by a 1,500-hp variable speed motor and consists of an inlet guide vane and four identical stages designed for accurate low-speed simulation of the rear stages of a high-speed core compressor. With reference to Fig. 3, the first two stages are used to set up a repeating stage

environment. The third stage is the focus of research measurements, while the fourth stage acts as a buffer to the exit conditions. The flow path has an outer diameter of 1.219 m and a hub-tip radius ratio of 0.80. The nominal rotor tip and stator seal clearances are 1.4% and 0.6% of span respectively. Rotor tip speed is 61 m/sec and nominal axial velocity is on the order of 25 m/sec. The flow control stator vanes located in the third stage are designed by applying modified NACA 65-series thickness distributions to modified circular-arc mean lines.

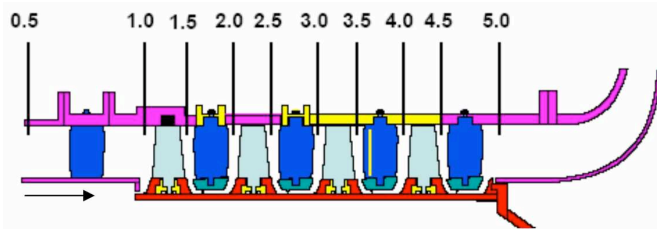


Fig. 3 - Compressor Stages

In order to implement this flow control concept, an effective feedback control strategy must be employed. Moreover, the flow control strategy must be capable of a real-time execution in a gas turbine engine operating environment. A prevailing method in the flow control research is based on the Moore-Greitzer model,<sup>6</sup> which is widely used to study stall control. This model is a three-state model for a compression system based on a single mode Galerkin projection. The problem with the Moore-Greitzer model remains that it is based on a reduced parametric model of compressor stall dynamics whose parameters are difficult to estimate due to highly complex stall flow. Furthermore, the Moore-Greitzer model is based on incompressible flow and does not address the intermediate flow along a compressor cascade. In this paper, we present a feedback adaptive flow control design using a physics-based distributed model based on the 1-D unsteady Euler equations for compressible flow. This model-based flow control can have a wide range of applicability beyond the immediate flow control problem in a compressor cascade. A loss parameter is incorporated into the Euler equations to represent the effect of the total pressure loss due to flow separation. The air injection mass flow control is formulated as a pointwise control within the interior region of the flow passage through the flow control vanes. An adjoint-based optimal control theory for the 1-D Euler model is developed for the flow control approach.

## II. Diffusion Concept

In diffusing flow, stall often occurs due to the presence of an adverse pressure gradient. Stall flow usually manifests itself as a reduced static pressure recovery and an increase in the total pressure loss.<sup>7</sup> Thus, the total pressure loss can be seen as an indicator for stall or flow separation. Lieblein showed that the stall onset relates to a parameter known as a diffusion factor which is well correlated with the boundary layer wake momentum thickness in the minimum-loss region of a 2-D compressor cascade.<sup>8</sup> A local diffusion factor  $D_{loc}$  is defined as the ratio of the velocity difference between the maximum velocity  $V_{max}$  and the outlet velocity  $V_2$  to the maximum velocity on the suction surface

$$D_{loc} = \frac{V_{max} - V_2}{V_{max}} \quad (1)$$

Typically, a detail knowledge of the velocity distribution on a compressor blade section is usually not known, so Lieblein alternatively defined a more convenient form of the diffusion factor based on the inlet and outlet velocities of the cascade according to

$$D = \left(1 - \frac{V_2}{V_1}\right) + \frac{\Delta V_\theta}{2\sigma V_1} \quad (2)$$

where  $D$  is the diffusion factor,  $\sigma$  is the solidity,  $\Delta V_\theta$  is the change in the tangential velocity through the cascade, and the subscripts 1 and 2 denote the inlet and outlet condition, respectively.

For an incompressible 2-D cascade, Eq. (2) becomes

$$D = \left(1 - \frac{\cos\beta_1}{\cos\beta_2}\right) + \frac{\cos\beta_1}{2\sigma} (\tan\beta_1 - \tan\beta_2) \quad (3)$$

where  $\beta$  is the air angle.

A theoretical analysis of incompressible 2-D cascade total pressure loss<sup>8</sup> shows that the wake momentum thickness  $\theta^*$  correlates well the the total pressure loss coefficient  $\bar{\omega}_1$  based on the inlet condition according to the relationship

$$\bar{\omega}_1 = \frac{p_{0,1} - p_{0,2}}{p_{0,1} - p_1} = 2 \left( \frac{\theta^*}{c} \right)_2 \frac{\sigma}{\cos\beta_2} \left( \frac{\cos\beta_1}{\cos\beta_2} \right)^2 \left\{ \frac{\frac{2H_2}{3H_2-1}}{\left[ 1 - \left( \frac{\theta^*}{c} \right)_2 \frac{\sigma H_2}{\cos\beta_2} \right]^3} \right\} \quad (4)$$

where  $p_0$  is the total pressure,  $\theta^*/c$  is the ratio of the wake momentum thickness to blade chord, and  $H_2$  is the wake form factor.

Hence, an increase in the wake momentum thickness resulting from flow separation in the cascade directly translates into an accompanied increase in the total pressure loss. Fig. 4 obtained from NASA SP-36 report<sup>8</sup> illustrates the diffusion factor correlation for a NACA 65-(A<sub>10</sub>)10 low-speed compressor cascade .

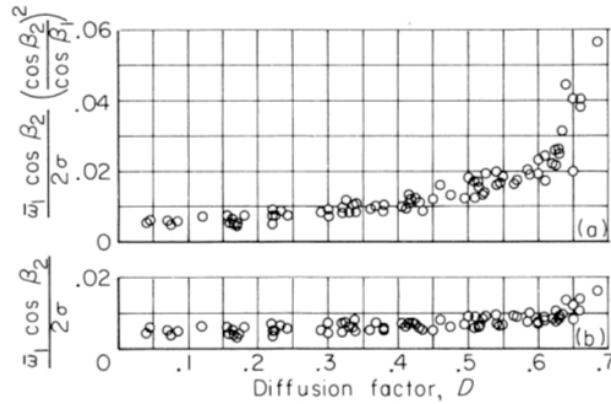


Fig. 4 - Diffusion Factor Correlation

As illustrated in Fig. 4, the diffusion factor is correlated well with the total pressure loss coefficient as defined in Eq. (4). Lieblein showed that the total pressure loss coefficient is generally a reliable indicator of the momentum thickness of the boundary layer formed over the blade surface. Thus, the larger the total pressure loss coefficient is, the thicker the boundary layer becomes. It is generally accepted that the stall onset occurs at about a diffusion factor of about 0.55 where the total pressure loss begins to increase rapidly<sup>8</sup> due to the thickening of the boundary layer, as can be seen in Fig. 4.

Based on the diffusion concept, it is reasonable to say that controlling flow separation is tantamount to controlling the total pressure loss. The most direct effect of this total pressure loss control is an increase in the static pressure recovery in a diffusing flow through the stator cascade. More importantly, this control also brings about a reduction in the boundary layer thickness, which therefore increases the turning angle and hence decreases the angle of attack on the rotor blade row to alleviate the stall flow on the rotor.

Thus, in a compressor environment, the total pressure measurement across a blade row can provide an indication of the potential stall onset. Typically, designers should know the design total pressure loss across a blade row, which could also be measured directly by running the compressor at the design point. When operating substantially above this design value, for example twice the design loss, an inference could be made about a probable flow separation event in the compressor that needs to be corrected. Flow control vanes can then be activated to inject bleed air into the flow passage in order to bring about a reduction in the total pressure loss.

### III. Adaptive Flow Control Architecture

In this study, a model-based flow control approach is proposed for controlling the total pressure loss across a stator cascade equipped with flow control vanes. The flow control architecture incorporates an adaptive parameter estimation that can estimate on-line the relationship between the air injection mass flow and the total pressure loss under varying engine operating environment. To minimize errors in the parameter estimation during the initial phase of estimation, CFD modeling will be used to provide data for an off-line estimation. While CFD technologies has been advancing

rapidly in many facets of fluid dynamics applications including turbomachinery, the complex nature of flow separation still pose a significant challenge in estimating total pressure losses in a compressor cascade using CFD modeling alone. Nonetheless, CFD modeling can greatly complement the limited knowledge obtained from experimentation to provide a more complete understanding of the flow characteristics. An effective flow control architecture therefore should incorporate both CFD modeling as well as experimental data in its design by leveraging the complementary nature of analytical and experimental methods.

Realizing that the flow environment in a compressor stage within a gas turbine engine can be quite complex, any flow control concept cannot possibly address all the subtlety of the real flow details in an actual gas turbine engine. Therefore, while the proposed flow control concept based on the 1-D Euler model may appear to overly simplify the real flow inside a compressor cascade, the incorporation of the parameter estimation into the flow control architecture is designed to complement the analytical model with real data from the gas turbine engine as an attempt to address the real flow problem. This approach is equivalent to the design process of a compressor which traditionally can be performed with simplified mathematical modeling combined with cascade empirical correlations to accurately estimate the velocity distribution within the cascade.

The road map for this fundamental research is to initially develop the proposed flow control concept that can be implemented in the LSAC test facility for demonstration of its feasibility. While the LSAC compressor is a low-speed compressor, it shares a number of similar features with the low-pressure compressor spool in a modern gas turbine engine, including a high hub-to-tip ratio and a high blade loading design, that make it a suitable flow control research environment for gas turbine engines. This would potentially facilitate the technology transition into gas turbine engines at the end of the research phase.

Fig. 5 illustrates a simplified block diagram of a flow control architecture which comprises three major features:

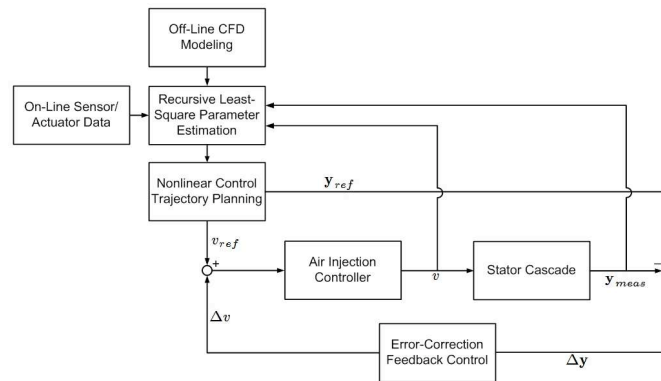


Fig. 5 - Flow Control Architecture

1. A *recursive least-square parameter estimator* is incorporated into the flow control architecture in order to estimate a total pressure loss parameter that relates the air injection mass flow and the total pressure loss. The total pressure loss data are obtained from experimental testing in the LSAC test facility at NASA Glenn Research Center. Additionally, a CFD modeling will be performed to provide total pressure loss data at various different air injection mass flow values and compressor configurations that were not available from experimental data. The CFD data will then be used for an initial off-line estimation of the air injection control effect on the total pressure loss. During an actual engine operation, as data become available from actual pressure, temperature, and flow sensors and air injection control actuator, the recursive least-square estimator continues to improve the accuracy of the model parameter. The parameter estimation therefore allows the controller to be adaptive to different engine conditions than anticipated and also to be better responsive to system uncertainties.
2. A *nonlinear trajectory optimization* is designed to provide a tracking control for maintaining a given target total pressure at the outlet of the stator cascade. The trajectory optimization is based on an adjoint method for the 1-D Euler equations with an interior pointwise control input that represents the air injection mass flow. This nonlinear optimization can be performed on-line based on a set point input to provide a gain schedule for the air injection mass flow. A second-order gradient method is implemented to perform this nonlinear trajectory optimization.

3. *An error-correction feedback optimal control* is designed to provide a corrective control that will minimize the error signals between the model output from the nonlinear trajectory optimization and the actual measurements of the total pressure at the outlet of the stator cascade. This corrective control is necessary in order to correct for modeling errors and changing inlet flow conditions which can cause a deviation in the trajectory, hence an error in the target total pressure.

From the instrumentation standpoint, the flow control architecture will utilize pressure and temperature sensors at both the inlet and outlet to actively monitor changes in the total pressure loss parameter. When the control system detects a total pressure loss parameter increasing beyond an allowable threshold, it will dispatch a command to raise the total pressure at the outlet to a desired value so as to maintain the total pressure loss to within an acceptable limit.

#### IV. 1-D Curvilinear Unsteady Flow Model

Flow through a compressor cascade is generally unsteady, viscous, and three dimensional as the flow field varies in both the meridional and tangential planes. In addition to the main flow in the inviscid core, significant secondary flow fields near the hub and tip regions also exist. Local flow fields around blade sections resulting from the potential effect at the leading edge and the wake effect at the trailing edge create tangential variations in the global flow field. Turbomachinery flow therefore is a very complex problem to analyze. In spite of the complexity, traditional compressor design methodologies often rely on simplified analyses that address the dominant features of the flow field. Secondary effects such as boundary layer blockage, tip clearance flow, and viscous losses are addressed in the design processes by simplified analytical and/or empirical methods. One such simplification is to ignore the flow field tangential variation in the bladeless region, thereby resulting in an axisymmetric flow field assumption which has been frequently used in the compressor design processes.<sup>9</sup> The flow properties in an axisymmetric flow field therefore can be interpreted in a circumferential average sense. Another simplification for compressors with slightly varying end wall diameters is by neglecting the radial flow effect.

In the current flow control concept, the air injection slots admit equal mass flow that depends on sensing at a particular radial station along the flow control vanes such as the tip radius where the viscous loss is most severe. Pressure loss information at this blade station is then used in the control design for the air injection. Thus, for this application, we can restrict the flow field on a cylindrical surface by neglecting the radial flow field effect. The flow field therefore varies in the axial and tangential directions. While this flow field can be computed by solving the Navier-Stokes equations using computational fluid dynamics (CFD) methods, the computational speed for even a 2-D flow is not sufficiently fast for a typical real-time demand in flow control applications. Therefore, reduced-order modeling has been frequently used in flow control applications<sup>10</sup> in recognition that a reduced fidelity of the flow field modeling can be traded for an increase in the computational speed. Moreover, the detail computed 2-D flow field around the flow control vanes would tend to provide information that cannot be directly correlated with the flow control experiment since the measured total pressure losses are usually based on their tangential average values, which are commonly used in determining a compressor cascade performance based on the diffusion factor concept.

Fig. 6 illustrates a 2-D flow through a compressor cascade wherein the stagnation streamlines in effect form a curved, diffusing flow passage through the compressor cascade. In this study, we propose a reduced-order model of this flow field using the 1-D curvilinear unsteady flow Euler equations with a total pressure loss parameter that accounts for the viscous dissipation of a real fluid caused by flow separation. This parameter is estimated by a parameter estimation process as a function of the air injection mass flow control, so in effect this parameter provides a means to reconcile the analytical model with experimental data. The 1-D curvilinear flow field thus represents an average flow through the cascade at any given cross section normal to the flow. For 1-D unsteady flow, we formulate the following Euler equations comprising the continuity, momentum, and energy equations in the conservation form with a pointwise control<sup>11</sup>

$$\mathbf{U}_t + \mathbf{F}(\mathbf{U})_x + \mathbf{Q}(\mathbf{U}, x, v) = \mathbf{0} \quad (5)$$

with

$$\mathbf{U} = \begin{bmatrix} \rho A \\ \rho u A \\ \rho A \left( e + \frac{1}{2} u^2 \right) \end{bmatrix}, \quad \mathbf{F}(\mathbf{U}) = \begin{bmatrix} \rho u A \\ \rho u^2 A + p A \\ \rho u A \left( e + \frac{1}{2} u^2 \right) + p u A \end{bmatrix}, \quad \mathbf{Q}(\mathbf{U}, x, v) = \begin{bmatrix} 0 \\ -p \frac{dA}{dx} + \frac{1}{2} \rho u^2 A \frac{\xi(x, v)}{L} \\ 0 \end{bmatrix}$$

where  $\rho$  is the density,  $p$  is the pressure,  $u$  is the flow speed,  $e$  is the specific internal energy,  $A(x)$  is the normal flow

area as a function of the position  $x$ ,  $L$  is the flow passage length, and  $\xi$  is the total pressure loss parameter as a function of the interior pointwise air injection mass flow control  $v(t)$  as well as the curvilinear coordinate  $x$ .

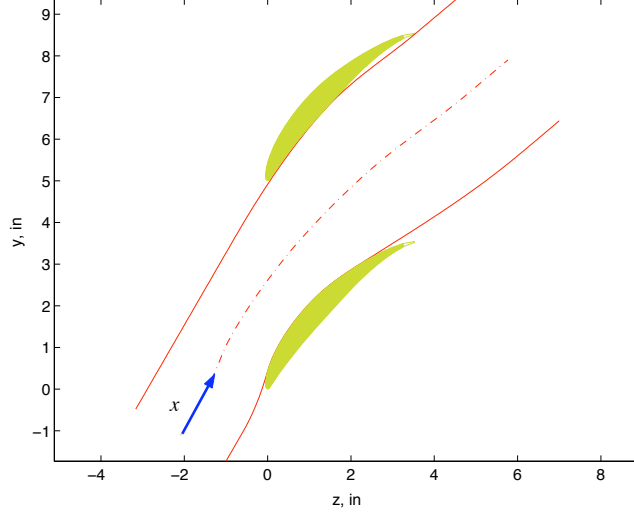


Fig. 6 - Flow Through a Compressor Cascade

The function  $\mathbf{F}$  is a flux function of the conserved variables, namely, mass flux, momentum flux, and energy flux. The function  $\mathbf{Q}$  is a non-homogeneous source term due to the viscous dissipation as well as the area change. The air injection mass flow control variable  $v$  exists at a single location on the suction surface within the cascade flow passage. Therefore, we refer to this type of control as an interior pointwise control. For subsonic flow, the non-conservation form of the Euler equations can be used alternatively in terms of the three typical performance variables in a compressor, namely, the mass flow  $\dot{m} = \rho u A$ , the total pressure  $p_0$ , and the total temperature  $T_0$  according to

$$\mathbf{y}_t + \mathbf{A}(\mathbf{y}, x) \mathbf{y}_x + \mathbf{B}(\mathbf{y}, x) \xi(x, v) = \mathbf{0} \quad (6)$$

where  $\mathbf{y}(x, t) = \begin{bmatrix} \dot{m} & p_0 & T_0 \end{bmatrix}^T$  is a vector of flow variables and

$$\mathbf{A} = \begin{bmatrix} u & \frac{pA}{\rho_0} & \frac{\dot{m}u}{2T_0} \\ \frac{\rho_0 c^2}{\rho A} & u \left[ 1 - \frac{(\gamma-1)T}{T_0} \right] & \frac{\rho_0 c^2 u}{T_0} \\ \frac{(\gamma-1)T}{\rho A} & -\frac{(\gamma-1)^2 T u}{k p_0} & u \left[ 1 + \frac{(\gamma-1)T}{T_0} \right] \end{bmatrix}, \quad \mathbf{B} = \begin{bmatrix} \frac{\dot{m}u}{2L} \\ \frac{\rho_0 u^3}{2L} \left( \frac{T_0}{T} - \gamma + 1 \right) \\ -\frac{(\gamma-1)uT}{L} \left( \frac{T_0}{T} - 1 \right) \end{bmatrix}$$

where, in addition to the previous definition,  $\rho_0$  is the total density,  $T$  is the temperature,  $c$  is the speed of sound, and  $\gamma$  is the specific heat ratio.

The non-conservation form of the Euler equations is more convenient and hence preferred for the adjoint analysis in this study. Equation (6) in fact also preserves the conservation of mass and energy by observing that its steady state form is

$$\frac{d\mathbf{y}}{dx} = -\mathbf{A}^{-1}(\mathbf{y}, x) \mathbf{B}(\mathbf{y}, x) \xi(x, v) \Leftrightarrow \frac{d}{dx} \begin{bmatrix} \dot{m} \\ p_0 \\ T_0 \end{bmatrix} = - \begin{bmatrix} 0 \\ \frac{\gamma p_0 M^2 \xi}{2L} \\ 0 \end{bmatrix} \quad (7)$$

Equation (6) is classified as a quasilinear hyperbolic partial differential equation (PDE). The hyperbolicity comes from the fact that the eigenvalues of  $\mathbf{A}$  are real and distinct. In fact, it can be shown that  $\lambda(\mathbf{A}) = u, u \pm c$  are the eigenvalues, which are the wave propagation speeds in a fluid medium. Subsonic flow therefore involves two waves propagating downstream and one wave propagating upstream from the source. Since the flow information is propagated in both directions, data must exist at the two end point boundaries. Furthermore, the number of upstream and downstream boundary conditions must match the number of upstream and downstream wave speeds. This is known as the boundary condition compatibility. Accordingly, we need to impose appropriate boundary conditions for

this flow model based on the sign-definiteness of the eigenvalues. Let  $x = 0$  denote the coordinate at the cascade inlet, and  $x = L$  denote the coordinate at the outlet, then these boundary conditions may be specified as

$$\mathbf{F}\mathbf{y}(0, t) + (\mathbf{I} - \mathbf{F})\mathbf{y}(L, t) = \mathbf{G}(t) + \mathbf{I}_1^T v(t) \quad (8)$$

where the subscript  $T$  denotes a matrix transpose operation,  $\mathbf{I}$  is the identity matrix of size 3,  $\mathbf{I}_1$  is the first row vector of  $\mathbf{I}$ ,

$$\mathbf{F} = \begin{bmatrix} 0 & 0 & 0 \\ 0 & 1 & 0 \\ 0 & 0 & 1 \end{bmatrix}$$

and  $\mathbf{G}(t) = \begin{bmatrix} \dot{m}_{in} & p_{0,in} & T_{0,in} \end{bmatrix}^T$  is the inlet flow condition.

Equation (8) satisfies the boundary compatibility condition. We note that the boundary condition (8) specifies that the mass flow quantity at the outlet is equal to that at the inlet plus the air injection mass flow. We also impose an initial condition based on the flow initially at a steady state condition according to

$$\mathbf{y}(x, 0) = \mathbf{y}_0(x) \quad (9)$$

so that  $\mathbf{y}_0(x)$  is a solution of Eq. (7) with a compatible boundary condition

$$\mathbf{F}\mathbf{y}_0(0) + (\mathbf{I} - \mathbf{F})\mathbf{y}_0(L) = \mathbf{G}(0) + \mathbf{I}_1^T v(0) \quad (10)$$

Equations (6), (8), and (9) thus completely define the 1-D model of a through flow through a compressor cascade. An advantage of this 1-D model is that we can set up a flow control problem for multi-stage compressor cascade without requiring extensive computing resources and it allows experimental total pressure data to be incorporated directly into the analytical model via the total pressure loss parameter. For the current research, we will use this flow control model on a single stator row.

## V. Loss Parameter Estimation

The total pressure loss parameter  $\xi$  in Eq. (6) models the total pressure loss in the compressor cascade. For air injection control, we postulate that this total pressure loss parameter is a non-negative function of the air injection mass flow control variable  $v$  that would result in a lower total pressure loss than when the air injection is not active. Thus, we have the following equation

$$\xi(x, v) = \xi_0 - \Delta\xi(x, v) \geq 0 \quad (11)$$

where  $\xi_0$  is the baseline total pressure loss parameter without air injection control and  $0 \leq \Delta\xi \leq \xi_0$  is a total pressure loss reduction parameter due to air injection mass flow.

The baseline total pressure loss parameter is measured directly from the total pressure loss or estimated from a diffusion factor correlation as

$$\xi_0 = \frac{\ln \frac{p_{0,1}}{p_{0,2}}}{\int_0^L \frac{\gamma M^2}{2L} dx} \approx \bar{\omega}_1 = f(D) \quad (12)$$

Using this model, controlling flow through a cascade is tantamount to controlling the total pressure loss reduction parameter via the air injection mass flow input to reduce the total pressure loss through the cascade. Generally, this total pressure loss reduction parameter is not known a priori and must be estimated as a function of the air injection mass flow. The LSAC experimental data are used to establish the relationship between the air injection mass flow control and the total pressure loss parameter. The experimental data indicate that the total pressure loss parameter could be approximated as a quadratic function of the air injection mass flow control as shown in Fig. 7. The advantage of the quadratic relationship is that the control derivative is linear and therefore easier to implement in a nonlinear trajectory optimization process. More importantly, the quadratic relationship will enable an efficient optimization process to compute a nonlinear air injection mass flow control gain schedule. Hence, we select the following functional form for estimating the pressure loss relationship as a quadratic function of the interior pointwise air injection mass flow control variable  $v$

$$\frac{\Delta\xi(x, v)}{\Delta\xi_{max}} = \begin{cases} 0 & x < a, \forall v(t) \\ \frac{v(t)}{v_{sat}} \left[ 2 - \frac{v(t)}{v_{sat}} \right] & x \geq a, v(t) < v_{sat} \\ 1 & x \geq a, v(t) \geq v_{sat} \end{cases} \quad (13)$$

where  $x = a$  is the coordinate of the air injection location on the stator blade taken to be 35% of chord,  $v_{sat}$  is the saturation air injection mass flow taken to be about  $1.54 \times 10^{-4}$  slug/sec or 0.86% of the total mass flow.

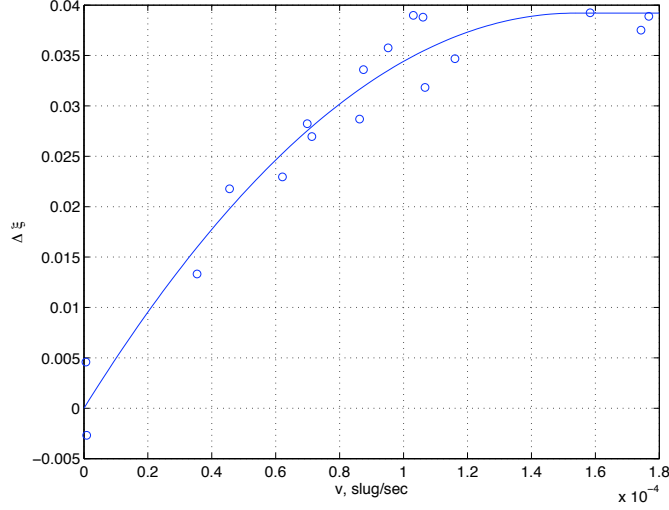


Fig. 7 - Total Pressure Loss Reduction Parameter Estimation

This model accounts for a control saturation when additional air injection beyond this value causes no further reduction in the total pressure loss. Also, the model assumes that the total pressure is unaffected upstream of the point of air injection on the stator blade. The initial estimate of the parameter  $\Delta\xi_{max}$  is computed to be 0.039 from an off-line least-square method using the LSAC test data as well as CFD data. The estimated functional relationship of the total pressure loss reduction parameter with the air injection mass flow is plotted in Fig. 7.

During an air injection flow control actuation, this parameter is continuously refined by a more efficient recursive least-square method which revises the new estimation incrementally using the results of the prior estimation. The equation of the recursive least-square method is<sup>12</sup>

$$\Delta\hat{\xi}_{max,i+1} = \Delta\hat{\xi}_{max,i} + (\mathbf{H}_i^T \mathbf{H}_i)^{-1} \mathbf{H}_{i+1}^T \left[ \mathbf{H}_{i+1} (\mathbf{H}_i^T \mathbf{H}_i)^{-1} \mathbf{H}_{i+1}^T \right]^{-1} \left( \mathbf{z}_{i+1} + \mathbf{H}_{i+1}^T \Delta\hat{\xi}_{max,i} \right) \quad (14)$$

where  $\mathbf{z} = \left[ \Delta\xi_1 \quad \Delta\xi_2 \quad \dots \quad \Delta\xi_n \right]^T$  and

$$\mathbf{H} = \begin{bmatrix} \frac{v_1}{v_{sat}} \left( 2 - \frac{v_1}{v_{sat}} \right) \\ \frac{v_2}{v_{sat}} \left( 2 - \frac{v_2}{v_{sat}} \right) \\ \vdots \\ \frac{v_n}{v_{sat}} \left( 2 - \frac{v_n}{v_{sat}} \right) \end{bmatrix}$$

The idea is to start out the air injection control using an initial estimate of the total pressure loss reduction parameter. The nonlinear trajectory optimization computes an initial air injection control trajectory for flow control implementation. After a predetermined  $n$  number of time steps, the computation uses the recently available total pressure loss data and the air injection mass flow input at the previous  $n$  time steps to revise the initial estimate of the total pressure loss reduction parameter using the recursive least-square method. The nonlinear trajectory optimization then uses this newly revised parameter and computes a revised air injection control trajectory. This process is then repeated for every  $n$  numbers of time steps until a desired total pressure at the outlet is achieved. A similar process can also be implemented in the error-correction feedback using the deviation of the estimated parameter.

## VI. Adjoint-Based Trajectory Optimization

A trajectory optimization is developed to compute a control gain schedule for the air injection control to achieve a total pressure set point at the outlet. Since fluid flow is governed by the nonlinear Euler equations, the trajectory

optimization is a nonlinear programming optimal control problem. Optimal control of distributed systems modeled by PDEs such as the Euler equations is a current subject of many mathematical research. In fluid problems, one approach is to transform the Euler equations into a system of ODEs by means of numerical discretization techniques such as finite-difference methods<sup>17</sup> or finite-element methods.<sup>13</sup> Discrete adjoint equations are then formulated for this discretized system. Another approach is to obtain continuous adjoint equations directly from the Euler equations via optimality conditions. This approach enjoys a considerable popularity in the aerodynamic shape optimization studies involving the Euler and Navier-Stokes equations.<sup>14</sup> The continuous adjoint approach is generally preferred over the discrete adjoint approach for Navier-Stokes flow problems.<sup>15</sup> In this study, we present a continuous adjoint method for a time-based optimization of the 1-D unsteady Euler equations. This is a significant difference from the adjoint approaches used for the aerodynamic shape optimization.<sup>14,15</sup>

For the problem at hand, we would like to minimize the following linear-quadratic cost function with a fixed terminal time  $t_f$  subject to Eqs. (5)-(9):

$$J = \frac{1}{2} \int_0^{t_f} \left\{ [\mathbf{y}(L, t) - \mathbf{y}_d(L)]^T \mathbf{I}_2^T Q \mathbf{I}_2 [\mathbf{y}(L, t) - \mathbf{y}_d(L)] + R(v - v_d)^2 \right\} dt \quad (15)$$

where  $Q \geq 0$  and  $R > 0$  are some weighting factors,  $\mathbf{I}_2$  is the second row vector of  $\mathbf{I}$  such that  $\mathbf{I}_2 \mathbf{y}(L, t) = p_0(L, t)$ , and  $\mathbf{I}_2 \mathbf{y}_d(L) = p_{0,d}(L)$  and  $v_d \leq v_{sat}$  are the desired total pressure set point at the outlet and the corresponding air injection mass flow control computed from the steady state Euler equations

$$\mathbf{A}(\mathbf{y}_d, x) \frac{d\mathbf{y}_d}{dx} + \mathbf{B}(\mathbf{y}_d, x) \xi(x, v_d) = \mathbf{0} \quad (16)$$

The necessary conditions for optimality of this system can be obtained from the variational principle. To that end, we now introduce the following dual Hamiltonian system<sup>16</sup>

$$H_1(\mathbf{y}, x, v, \boldsymbol{\lambda}) = -\boldsymbol{\lambda}^T \mathbf{B} \xi(x, v) \quad (17)$$

$$H_2(\mathbf{y}(0, t), \mathbf{y}(L, t), v, \boldsymbol{\eta}) = \frac{1}{2} [\mathbf{y}(L, t) - \mathbf{y}_d(L)]^T \mathbf{I}_2^T Q \mathbf{I}_2 [\mathbf{y}(L, t) - \mathbf{y}_d(L)] + \frac{1}{2} R(v - v_d)^2 + \boldsymbol{\eta}^T [\mathbf{F} \mathbf{y}(0, t) + (\mathbf{I} - \mathbf{F}) \mathbf{y}(L, t) - \mathbf{G} - \mathbf{I}_1^T v] \quad (18)$$

where  $\boldsymbol{\lambda}(x, t)$  is a continuous adjoint vector for Eq. (6) and  $\boldsymbol{\eta}(t)$  is an adjoint vector for the boundary condition (8).

Then the augmented cost function becomes

$$J = \int_0^{t_f} \int_0^L [H_1 - \boldsymbol{\lambda}^T (\mathbf{y}_t + \mathbf{A} \mathbf{y}_x)] dx dt + \int_0^{t_f} H_2 dt \quad (19)$$

We compute the first variation of the cost function  $J$  as

$$\delta J = \int_0^{t_f} \int_0^L [H_{1,\mathbf{y}} \delta \mathbf{y} + H_{1,v} \delta v - \boldsymbol{\lambda}^T (\delta \mathbf{y}_t + \mathbf{A} \delta \mathbf{y}_x + \mathbf{A}_\mathbf{y} \mathbf{y}_x \delta \mathbf{y})] dx dt + \int_0^{t_f} [H_{2,\mathbf{y}(0,t)} \delta \mathbf{y}(0, t) + H_{2,\mathbf{y}(L,t)} \delta \mathbf{y}(L, t) + H_{2,v} \delta v] dt \quad (20)$$

Invoking the Green's theorem yields

$$\iint_{\Omega} \boldsymbol{\lambda}^T (\delta \mathbf{y}_t + \mathbf{A} \delta \mathbf{y}_x + \mathbf{A}_\mathbf{y} \mathbf{y}_x \delta \mathbf{y}) dx dt = - \iint_{\Omega} (\boldsymbol{\lambda}_t^T + \boldsymbol{\lambda}_x^T \mathbf{A} + \boldsymbol{\lambda}^T \mathbf{A}_x) \delta \mathbf{y} dx dt + b \quad (21)$$

where the boundary condition term  $b$  is computed by integrating the contour integral on the boundary  $\Gamma$  with zero variations of  $b$  at  $x = 0$  and  $t = 0$

$$b = \oint_{\Gamma} (\boldsymbol{\lambda}^T \mathbf{A} \delta \mathbf{y} dt - \boldsymbol{\lambda}^T \delta \mathbf{y} dx) = \int_0^{t_f} \left[ \boldsymbol{\lambda}^T(L, t) \mathbf{A}(\mathbf{y}(L, t), L) \delta \mathbf{y}(L, t) - \boldsymbol{\lambda}^T(0, t) \mathbf{A}(\mathbf{y}(0, t), 0) \delta \mathbf{y}(0, t) \right] dt + \int_0^L \boldsymbol{\lambda}^T(x, t_f) \delta \mathbf{y}(x, t_f) dx \quad (22)$$

Using the foregoing results, the first variation of the cost function  $J$  becomes

$$\begin{aligned} \delta J = & \int_0^{t_f} \int_0^L \left[ (H_{1,y} + \lambda_t^T + \lambda_x^T \mathbf{A} + \lambda^T \mathbf{A}_x) \delta \mathbf{y} + H_{1,v} \delta v \right] dx dt - \int_0^L \lambda^T(x, t_f) \delta \mathbf{y}(x, t_f) dx \\ & - \int_0^{t_f} \left[ \lambda^T(L, t) \mathbf{A}(\mathbf{y}(L, t), L) \delta \mathbf{y}(L, t) - \lambda^T(0, t) \mathbf{A}(\mathbf{y}(0, t), 0) \delta \mathbf{y}(0, t) \right] dt \\ & + \int_0^{t_f} \left[ H_{2,y(0,t)} \delta \mathbf{y}(0, t) + H_{2,y(L,t)} \delta \mathbf{y}(L, t) + H_{2,v} \delta v \right] dt dx \quad (23) \end{aligned}$$

Necessary conditions for optimality for a relative minimum of the cost function  $J$  require that its first variation be zero for any arbitrary admissible variation. As a result, we obtain the following adjoint equation and split boundary conditions

$$\lambda_t + (\mathbf{A}^T \lambda)_x + H_{1,y}^T = \mathbf{0} \quad (24)$$

$$\mathbf{A}^T(\mathbf{y}(0, t), 0) \lambda(0, t) + H_{2,y(0,t)}^T = \mathbf{0} \quad (25)$$

$$\mathbf{A}^T(\mathbf{y}(L, t), L) \lambda(L, t) - H_{2,y(L,t)}^T = \mathbf{0} \quad (26)$$

Equations (25) and (26) can be expanded as

$$\mathbf{A}^T(\mathbf{y}(0, t), 0) \lambda(0, t) + \mathbf{F}^T \boldsymbol{\eta} = \mathbf{0} \quad (27)$$

$$\mathbf{A}^T(\mathbf{y}(L, t), L) \lambda(L, t) - (\mathbf{I} - \mathbf{F}^T) \boldsymbol{\eta} - \mathbf{I}_2^T Q \mathbf{I}_2 [\mathbf{y}(L, t) - \mathbf{y}_d(L)] = \mathbf{0} \quad (28)$$

Subtracting Eqs. (28) from (27) gives

$$\boldsymbol{\eta} = -\mathbf{A}^T(\mathbf{y}(0, t), 0) \lambda(0, t) + \mathbf{A}^T(\mathbf{y}(L, t), L) \lambda(L, t) - \mathbf{I}_2^T Q \mathbf{I}_2 [\mathbf{y}(L, t) - \mathbf{y}_d(L)] \quad (29)$$

Upon simplification, the adjoint equation can be written as

$$\lambda_t + (\mathbf{A}^T \lambda)_x - \mathbf{B}_y^T \xi(x, v) \lambda = \mathbf{0} \quad (30)$$

subject to the following boundary and terminal-time conditions

$$(\mathbf{I} - \mathbf{F}^T) \mathbf{A}^T(\mathbf{y}(0, t), 0) \lambda(0, t) + \mathbf{F}^T \mathbf{A}^T(\mathbf{y}(L, t), L) \lambda(L, t) = \mathbf{F}^T \mathbf{I}_2^T Q \mathbf{I}_2 [\mathbf{y}(L, t) - \mathbf{y}_d(L)] \quad (31)$$

$$\lambda(x, t_f) = \mathbf{0} \quad (32)$$

From the optimality conditions, we also obtain an optimal control for the air injection mass flow as

$$\int_0^L H_{1,v}^T dx + H_{2,v}^T = 0 \quad (33)$$

This can also be written as

$$\frac{2\Delta\xi_{max}}{v_{sat}} \left( 1 - \frac{v}{v_{sat}} \right) \int_0^L \mathbf{B}^T \lambda dx + R(v - v_d) + \mathbf{I}_1 [\mathbf{A}^T(\mathbf{y}(0, t), 0) \lambda(0, t) - \mathbf{A}^T(\mathbf{y}(L, t), L) \lambda(L, t)] = 0 \quad (34)$$

for  $x \geq a$  and  $v(t) < v_{sat}$ .

Using the functional relationship in the parameter estimation, the optimal air injection mass flow control can be directly solved in terms of the adjoint vector  $\lambda(x, t)$

$$v = \text{sat}(v_{opt}) = \begin{cases} 0 & v \leq 0 \\ v_{opt} & 0 < v < v_{sat} \\ v_{sat} & v \geq v_{sat} \end{cases} \quad (35)$$

where

$$v_{opt}(t) = v_d - \frac{\frac{2\Delta\xi_{max}}{v_{sat}} \left(1 - \frac{v_d}{v_{sat}}\right) \int_0^L \mathbf{B}^T \boldsymbol{\lambda} dx + \mathbf{I}_1 [\mathbf{A}^T(\mathbf{y}(0,t), 0) \boldsymbol{\lambda}(0,t) - \mathbf{A}^T(\mathbf{y}(L,t), L) \boldsymbol{\lambda}(L,t)]}{R - \frac{2\Delta\xi_{max}}{v_{sat}^2} \int_0^L \mathbf{B}^T \boldsymbol{\lambda} dx} \quad (36)$$

Equation (36) is the optimal control solution for the interior pointwise air injection mass flow control. It depends on the solution of the continuous adjoint vector  $\boldsymbol{\lambda}(x, t)$ , which would require solving the adjoint equation (30) with its terminal-time and boundary conditions (32) and (31). We see that in order to ensure a non-singular optimal control solution, we require that

$$R \neq \frac{2\Delta\xi_{max}}{v_{sat}^2} \int_0^L \mathbf{B}^T \boldsymbol{\lambda} dx \quad (37)$$

Since  $\boldsymbol{\lambda}(x, t_f) = \mathbf{0}$ , then the optimal control will converge to the desired air injection mass flow control as  $t \rightarrow t_f$ . We also want to ensure that the desired air injection mass flow control is not too close to the saturation value since the control will not be as effective beyond this value.

## VII. Computational Method

To compute the air injection optimal control trajectory, we implement a Newton-Raphson or second-order gradient method. First, we assume an initial but arbitrary control trajectory. Using this control, we proceed to solve a two-point boundary value problem involving the Euler and adjoint equations using a wave-splitting, explicit-scheme, finite-difference upwind method.<sup>17</sup> The new update on the control trajectory can then be computed from Eq. (36). The whole iterative process is repeated until a convergence on the control trajectory is achieved.

A general gradient method is given as

$$v^{k+1} = v^k - \varepsilon^k H_v^k \quad (38)$$

where  $k$  denotes the  $k$ -th iteration,  $0 \leq \varepsilon \leq 1$  is the update weight, and

$$H_v = \int_0^L H_{1,v}^T dx + H_{2,v}^T \quad (39)$$

To implement a second-order gradient method, we set

$$\varepsilon = H_{vv}^{-1} \quad (40)$$

where  $H_{vv}$  is the Hessian of the Hamiltonian with respect to the control, which is evaluated as

$$H_{vv} = \int_0^L H_{1,vv}^T dx + H_{2,vv}^T = R - \frac{2\Delta\xi_{max}}{v_{sat}^2} \int_0^L \mathbf{B}^T \boldsymbol{\lambda} dx \quad (41)$$

To solve for the optimal control in the gradient method, we need to compute the continuous adjoint vector  $\boldsymbol{\lambda}(x, t)$ , which in turn requires the solution of  $\mathbf{y}(x, t)$ . Thus, both Eqs. (6) and (30) and their associated initial or terminal-time and boundary conditions must be solved simultaneously. We implement the solutions of the Euler and adjoint equations using a wave-splitting, explicit-scheme finite-difference upwind method. To that end, we assume that the flow is entirely subsonic. Then, the eigenvalues of the matrix  $\mathbf{A}$  have mixed signs. The matrix  $\mathbf{A}$  can then be splitted into a semi-positive definite matrix and a semi-negative definite matrix as

$$\mathbf{A} = \mathbf{A}^+ + \mathbf{A}^- \quad (42)$$

where

$$\begin{aligned} \mathbf{A}^+ &= \boldsymbol{\Phi} \boldsymbol{\Lambda}^+ \boldsymbol{\Phi}^{-1} \\ \mathbf{A}^- &= \boldsymbol{\Phi} \boldsymbol{\Lambda}^- \boldsymbol{\Phi}^{-1} \end{aligned}$$

with  $\boldsymbol{\Phi}$  a matrix of right eigenvectors and

$$\boldsymbol{\Lambda}^+ = \begin{bmatrix} u+c & 0 & 0 \\ 0 & u & 0 \\ 0 & 0 & 0 \end{bmatrix} \geq \mathbf{0}, \quad \boldsymbol{\Lambda}^- = \begin{bmatrix} 0 & 0 & 0 \\ 0 & 0 & 0 \\ 0 & 0 & u-c \end{bmatrix} \leq \mathbf{0}$$

Equation (6) can be written in a wave-splitting characteristic form as

$$\Phi^{-1} \mathbf{y}_t + \Lambda^+ \Phi^{-1} \mathbf{y}_x + \Lambda^- \Phi^{-1} \mathbf{y}_x + \Phi^{-1} \mathbf{B} \xi = \mathbf{0} \quad (43)$$

Equation (43) is now discretized using a first-order finite-difference upwind method as

$$\Phi^{-1} \dot{\mathbf{y}}_i + \Lambda^+ \Phi^{-1} \frac{\mathbf{y}_i - \mathbf{y}_{i-1}}{\Delta x} + \Lambda^- \Phi^{-1} \frac{\mathbf{y}_{i+1} - \mathbf{y}_i}{\Delta x} + \Phi^{-1} \mathbf{B} \xi = \mathbf{0} \quad (44)$$

where  $i = 2, 3, \dots, m-1$  denotes the index of the interior points not on the boundary such that  $x_i = \frac{i-1}{m-1}L$  and  $\mathbf{y}_i(t) = \mathbf{y}(x_i, t)$ .

Eq. (44) can further be decomposed into three scalar equations corresponding to the three wave speeds as

$$(\Psi_1)_{i-1} \dot{\mathbf{y}}_i + (u_{i-1} + c_{i-1}) (\Psi_1)_{i-1} \frac{\mathbf{y}_i - \mathbf{y}_{i-1}}{\Delta x} + (\Psi_1)_{i-1} \mathbf{B}_{i-1} \xi_{i-1} = 0 \quad (45)$$

$$(\Psi_2)_{i-1} \dot{\mathbf{y}}_i + u_{i-1} (\Psi_2)_{i-1} \frac{\mathbf{y}_i - \mathbf{y}_{i-1}}{\Delta x} + (\Psi_2)_{i-1} \mathbf{B}_{i-1} \xi_{i-1} = 0 \quad (46)$$

$$(\Psi_3)_i \dot{\mathbf{y}}_i + (u_i - c_i) (\Psi_3)_i \frac{\mathbf{y}_{i+1} - \mathbf{y}_i}{\Delta x} + (\Psi_3)_i \mathbf{B}_i \xi_i = 0 \quad (47)$$

where  $(\Psi_k)_i$ ,  $k = 1, 2, 3$ , is the  $k$ -th  $1 \times 3$  row vector of the matrix  $\Phi^{-1}(\mathbf{y}_i, x_i)$ .

We now combine Eqs. (45) to (47) into a vector form as

$$\dot{\mathbf{y}}_i + \mathbf{A}_{i-1}^+ \frac{\mathbf{y}_i - \mathbf{y}_{i-1}}{\Delta x} + \mathbf{A}_i^- \frac{\mathbf{y}_{i+1} - \mathbf{y}_i}{\Delta x} + \mathbf{B}_{i-1}^+ \xi_{i-1} + \mathbf{B}_i^- \xi_i = \mathbf{0} \quad (48)$$

where

$$\begin{aligned} \mathbf{A}_{i-1}^+ &= \Psi^{-1} \Lambda_{i-1}^+ \Psi \\ \mathbf{A}_i^- &= \Psi^{-1} \Lambda_i^- \Psi \\ \mathbf{B}_{i-1}^+ &= \Psi^{-1} \begin{bmatrix} (\Psi_1)_{i-1} \\ (\Psi_2)_{i-1} \\ \mathbf{0}_{1 \times 3} \end{bmatrix}_{3 \times 3} \mathbf{B}_{i-1} \\ \mathbf{B}_i^- &= \Psi^{-1} \begin{bmatrix} \mathbf{0}_{1 \times 3} \\ \mathbf{0}_{1 \times 3} \\ (\Psi_3)_i \end{bmatrix}_{3 \times 3} \mathbf{B}_i \\ \Psi &= \begin{bmatrix} (\Psi_1)_{i-1} \\ (\Psi_2)_{i-1} \\ (\Psi_3)_i \end{bmatrix}_{3 \times 3} \end{aligned}$$

and  $\mathbf{0}_{1 \times 3}$  is the  $1 \times 3$  zero row vector.

At the incoming boundary  $x = 0$ , Eq. (44) cannot admit a positive wave which would require the solution to include a point upstream of  $x = 0$  that is nonexistent. Only the negative wave speed characteristic equation (47) is admitted. Using the Euler's method, we combine Eq. (47) with the boundary condition (8) so that

$$\mathbf{y}_{1,j+1} = \begin{bmatrix} (\Psi_3)_{1,j} \\ \mathbf{I}_2 \\ \mathbf{I}_3 \end{bmatrix}_{3 \times 3}^{-1} \begin{bmatrix} (\Psi_3)_{1,j} (\mathbf{y}_{1,j} - \Delta t \mathbf{B}_{1,j} \xi_{1,j}) - \frac{\Lambda_{1,j}^- \Delta t}{\Delta x} (\Psi_3)_{1,j} (\mathbf{y}_{2,j} - \mathbf{y}_{1,j}) \\ p_{0,in}(t_{j+1}) \\ T_{0,in}(t_{j+1}) \end{bmatrix}_{3 \times 1} \quad (49)$$

where the subscript  $j = 1, 2, \dots, n-1$  is the time index such that  $t_j = \frac{j-1}{n-1}t_f$ .

We next consider the boundary at  $x = L$ . The situation is now reverse whereby the solution can only admit the two positive eigenvalue characteristic equations (45) and (46). Combining with the boundary condition (8) yields

$$\mathbf{y}_{m,j+1} = \begin{bmatrix} \mathbf{I}_1 \\ (\Psi_1)_{m-1,j} \\ (\Psi_2)_{m-1,j} \end{bmatrix}_{3 \times 3}^{-1} \times \begin{bmatrix} \dot{m}_{in}(t_{j+1}) + v(t_{j+1}) \\ (\Psi_1)_{m-1,j} (\mathbf{y}_{m,j} - \Delta t \mathbf{B}_{m-1,j} \xi_{m-1,j}) - \frac{\Lambda_{m-1,j}^+ \Delta t}{\Delta x} (\Psi_1)_{m-1,j} (\mathbf{y}_{m,j} - \mathbf{y}_{m-1,j}) \\ (\Psi_2)_{m-1,j} (\mathbf{y}_{m,j} - \Delta t \mathbf{B}_{m-1,j} \xi_{m-1,j}) - \frac{\Lambda_{m-1,j}^+ \Delta t}{\Delta x} (\Psi_2)_{m-1,j} (\mathbf{y}_{m,j} - \mathbf{y}_{m-1,j}) \end{bmatrix}_{3 \times 1} \quad (50)$$

Thus, initially we guess a time history for the control  $v(t)$ . Equations (49) and (50) are then solved for the information on the boundary at the next time step. The interior points are then computed by integrating Eq. (48) forward in time. The complete time history of  $\mathbf{y}(x, t)$  based on the initial guess of the control  $v(t)$  is then used to solve the adjoint equation (30) for  $\lambda(x, t)$ . The control  $v(t)$  is then updated in the next iteration from the second-order gradient method, Eq. (38). This process is repeated until the solution of the control  $v(t)$  converges.

To solve for the adjoint vector  $\lambda(x, t)$ , it is convenient to cast the adjoint equation in a backward space and backward time formulation. We transform Eq. (30) by introducing distance-to-go variable  $\chi = L - x$  and time-to-go variable  $\tau = t_f - t$  and letting  $\varphi(\chi, \tau) = \lambda(x, t)$ . Then, Eq. (30) is rewritten as

$$\vartheta_t + \mathbf{A}^T \vartheta_x - \mathbf{C}^T \vartheta = 0 \quad (51)$$

where

$$\mathbf{C}^T = \mathbf{A}_x^T - \mathbf{B}_y^T \xi$$

We note that  $\mathbf{A}$  and  $\mathbf{C}$  depend on  $\mathbf{y}(x, t)$  and  $x$ , so Eq. (51) has both forward and backward space and time variables. Equation (51) can be solved using a similar wave-splitting finite-difference method. The resulting space-discretized equation is obtained as

$$\dot{\vartheta}_i + \mathbf{A}_{m-i+2}^{T+} \frac{\vartheta_i - \vartheta_{i-1}}{\Delta \chi} + \mathbf{A}_{m-i+1}^{T-} \frac{\vartheta_{i+1} - \vartheta_i}{\Delta \chi} - \mathbf{C}_{m-i+2}^{T+} \vartheta_{i-1} - \mathbf{C}_{m-i+1}^{T-} \vartheta_i = 0 \quad (52)$$

where

$$\begin{aligned} \mathbf{A}_{m-i+2}^{T+} &= (\Phi^T)^{-1} \Lambda_{m-i+2}^+ \Phi^T \\ \mathbf{A}_{m-i+1}^{T-} &= (\Phi^T)^{-1} \Lambda_{m-i+1}^- \Phi^T \\ \mathbf{C}_{m-i+2}^{T+} &= (\Phi^T)^{-1} \begin{bmatrix} (\Phi_1^T)_{m-i+2} \\ (\Phi_2^T)_{m-i+2} \\ \mathbf{0}_{1 \times 3} \end{bmatrix}_{3 \times 13} \mathbf{C}_{m-i}^T \\ \mathbf{C}_{m-i+1}^{T-} &= (\Phi^T)^{-1} \begin{bmatrix} \mathbf{0}_{1 \times 3} \\ \mathbf{0}_{1 \times 3} \\ (\Phi_3^T)_{m-i+1} \end{bmatrix}_{3 \times 3} \mathbf{C}_{m-i+1}^T \\ \Phi^T &= \begin{bmatrix} (\Phi_1^T)_{m-i+2} \\ (\Phi_2^T)_{m-i+2} \\ (\Phi_3^T)_{m-i+1} \end{bmatrix}_{3 \times 3} \end{aligned}$$

and  $(\Phi_k^T)_i$ ,  $k = 1, 2, 3$  are the  $k$ -th row vector of the matrix  $\Phi^T(\mathbf{y}_i, x_i)$ .

Similarly, the transformed boundary condition

$$(\mathbf{I} - \mathbf{F}^T) \mathbf{A}^T(\mathbf{y}(0, t), 0) \vartheta(L, \tau) + \mathbf{F}^T \mathbf{A}^T(\mathbf{y}(L, t), L) \vartheta(0, \tau) = \mathbf{F}^T \mathbf{I}_2^T \mathbf{Q} \mathbf{I}_2 [\mathbf{y}(L, t) - \mathbf{y}_d(L)] \quad (53)$$

can be solved as

$$\boldsymbol{\vartheta}_{1,j+1} = \begin{bmatrix} (\boldsymbol{\Phi}_3^T)_{m,n-j+1} \\ (\mathbf{A}_2^T)_{m,n-j+1} \\ (\mathbf{A}_3^T)_{m,n-j+1} \end{bmatrix}_{3 \times 3}^{-1} \times \begin{bmatrix} (\boldsymbol{\Phi}_3^T)_{m,n-j+1} (\boldsymbol{\vartheta}_{1,j} + \Delta\tau \mathbf{C}_{m,n-j+1}^T \boldsymbol{\vartheta}_{1,j}) - \frac{\Lambda_{m,n-j+1}^- \Delta\tau}{\Delta\chi} (\boldsymbol{\Phi}_3^T)_{m,n-j+1} (\boldsymbol{\vartheta}_{2,j} - \boldsymbol{\vartheta}_{1,j}) \\ Q[p_0(L, t_{n-j+1}) - p_{0,d}(L)] \\ 0 \end{bmatrix}_{3 \times 1} \quad (54)$$

$$\boldsymbol{\vartheta}_{m,j+1} = \begin{bmatrix} (\mathbf{A}_1^T)_{1,n-j+1} \\ (\boldsymbol{\Phi}_1^T)_{2,n-j+1} \\ (\boldsymbol{\Phi}_2^T)_{2,n-j+1} \end{bmatrix}_{3 \times 3}^{-1} \times \begin{bmatrix} 0 \\ (\boldsymbol{\Phi}_1^T)_{2,n-j+1} (\boldsymbol{\vartheta}_{m,j} + \Delta\tau \mathbf{C}_{2,n-j+1}^T \boldsymbol{\vartheta}_{m-1,j}) - \frac{\Lambda_{2,n-j+1}^- \Delta\tau}{\Delta\chi} (\boldsymbol{\Phi}_1^T)_{2,n-j+1} (\boldsymbol{\vartheta}_{m,j} - \boldsymbol{\vartheta}_{m-1,j}) \\ (\boldsymbol{\Phi}_2^T)_{2,n-j+1} (\boldsymbol{\vartheta}_{m,j} + \Delta\tau \mathbf{C}_{2,n-j+1}^T \boldsymbol{\vartheta}_{m-1,j}) - \frac{\Lambda_{2,n-j+1}^- \Delta\tau}{\Delta\chi} (\boldsymbol{\Phi}_2^T)_{m,n-j+1} (\boldsymbol{\vartheta}_{m,j} - \boldsymbol{\vartheta}_{m-1,j}) \end{bmatrix}_{3 \times 1} \quad (55)$$

where  $(\mathbf{A}_k^T)_{i,j}$ ,  $k = 1, 2, 3$  are the  $k$ -th row vector of the matrix  $\mathbf{A}^T(\mathbf{y}_i(t_j), x_i)$ .

Once the transformed adjoint vector  $\boldsymbol{\vartheta}(\chi, \tau)$  is computed, then the original adjoint vector  $\boldsymbol{\lambda}(x, t)$  can simply be determined by

$$\boldsymbol{\lambda}_{i,j} = \boldsymbol{\vartheta}_{m-i+1,n-j+1} \quad (56)$$

The Jacobian  $H_v$  and the Hessian  $H_{vv}$  can be evaluated by numerical integration using the known results of the adjoint vector  $\boldsymbol{\lambda}(x, t)$ . The results are then used to compute the next iteration of the control  $v$ . This iterative gradient method results in a rapid convergence usually within two iterations due to the linear-quadratic cost function and the assumed quadratic relationship of the air injection mass flow control. Because of the second-order convergence, the nonlinear trajectory optimization method can be adapted to a real-time computing of a desired air injection mass flow control trajectory.

The trajectory optimization solution generally provides an open-loop optimal control which can be used to command the air injection actuation. Using gain scheduling, the control can be turned into a feedback form based on the trajectory of the desired total pressure at the outlet. In practice, the open-loop control is not robust enough since disturbances or modeling errors will immediately destroy the optimality of the control, thereby causing the output to not achieve a desired value. Therefore, an error-correction linearized feedback must be incorporated into the overall flow control architecture to deal with system disturbances and uncertainties resulting from a gas turbine engine operating environment.

## VIII. Error-Correction Linear Feedback Optimal Control

The objective of the error-correction feedback is to compensate for modeling errors or aerodynamic variations in the inlet flow condition which act as a disturbance to the flow through the stator cascade. The nonlinear trajectory optimization computes the values of the reference flow variables  $\mathbf{y}(x, t)$  which are compared to the measured values. Error signals are then computed by subtracting the measured values from the reference values. Since the error signals should be small, the Euler equations can be linearized about the optimal control trajectory. The linear perturbation of the Euler equations is

$$\Delta \mathbf{y}_t + \mathbf{A} \Delta \mathbf{y}_x + \mathbf{A} \left[ \mathbf{A}^{-1} \mathbf{y}_t + (\mathbf{A}^{-1} \mathbf{B})_y \boldsymbol{\xi}(x, t) \right] \Delta \mathbf{y} + \mathbf{B} \boldsymbol{\xi}_v \Delta v = \mathbf{0} \quad (57)$$

We assume that the disturbances are manifested by changes in the inlet flow condition or modeling errors to cause the measured outputs to deviate from the reference trajectory. Since the mass flow and total temperature do not

vary significantly through the stator cascade due to the conservation of mass and energy, we can make a reasonable assumption that their gradients are constant. Then the linearized momentum component of the Euler equations can be approximated as

$$a_1(x, t) \Delta p_{0,t} + \Delta p_{0,x} + a_2(x, t) \Delta p_0 + a_3(x, t) \Delta v + a_4(x, t) \Delta \dot{m}_{in} + a_5(x, t) \Delta T_{0,in} = 0 \quad (58)$$

subject to the boundary condition

$$\Delta p_0(0, t) = \Delta p_{0,in} \quad (59)$$

The coefficients in Eq. (58) are computed from the reference mass flow  $\dot{m}$ , total pressure  $p_0$ , total temperature  $T_0$ , and the Mach number  $M$  on the optimal trajectory as

$$\begin{aligned} a_1 &= \frac{2 + (\gamma - 1) M^2}{4 - 2\gamma + (\gamma - 1) M^2} \frac{1}{u} > 0 \\ a_2 &= -\frac{\gamma M^2 (1 + \gamma M^2)}{2(1 - M^2)} \frac{\xi}{L} \\ a_3 &= -\gamma p_0 M^2 \frac{\Delta \xi_{max}}{L v_{sat}} \left(1 - \frac{v}{v_{sat}}\right) \\ a_4 &= \frac{\gamma p_0 M^2 (1 + \frac{\gamma-1}{2} M^2)}{\dot{m} (1 - M^2)} \frac{\xi}{L} \\ a_5 &= \frac{\gamma p_0 M^2 (1 + \frac{\gamma-1}{2} M^2)}{2T_0 (1 - M^2)} \frac{\xi}{L} \end{aligned}$$

From Eq. (58), we see that changes in the inlet mass flow  $\Delta \dot{m}_{in}$ , total pressure  $\Delta p_{0,in}$ , and total temperature  $\Delta T_{0,in}$  together act as disturbances to the total pressure error at the outlet. The objective of the feedback control therefore is to regulate the total pressure error at the stator outlet under the influence of these disturbances. To compute the feedback control, we introduce a new quasi-steady state feedback optimal control approach based on the adjoint method formulated in the previous section. We thus consider the following linear-quadratic cost function to minimize the total pressure error at the outlet and the corrective control action

$$J = \int_0^{t_f} \left[ \frac{1}{2} Q \Delta p_0^2(L, t) + \frac{1}{2} R \Delta v^2 \right] dt \quad (60)$$

where  $Q \geq 0$  and  $R > 0$ .

The adjoint of the linearized Euler equation is

$$\lambda_t + \left( \frac{\lambda}{a_1} \right)_x - \frac{a_2 \lambda}{a_1} = 0 \quad (61)$$

subject to the boundary condition:

$$\frac{\lambda(L, t)}{a_1(L, t)} = Q \Delta p_0(L, t) \quad (62)$$

The optimal control can be found from Eq. (33) as

$$R \Delta v - \int_0^L \frac{a_3 \lambda}{a_1} dx = 0 \quad (63)$$

To derive a feedback control, we now assume an adjoint solution in the form of a linear combination of the total pressure error, the corrective control, and the mass flow and total temperature disturbances

$$\frac{\lambda(x, t)}{a_1(x, t)} = P_1(x, t) \Delta p_0(x, t) + P_2(x, t) \Delta v(t) + P_3(x, t) \Delta \dot{m}_{in}(t) + P_4(x, t) \Delta T_{0,in}(t) \quad (64)$$

Substituting this into Eqs. (61) and (62) and neglecting the term  $\lambda_t$ , which in essence gives rise to a quasi-steady state solution, we obtain the following equation

$$\frac{\partial}{\partial x} \begin{bmatrix} P_1 \\ P_2 \\ P_3 \\ P_4 \end{bmatrix} = \begin{bmatrix} 2a_2 & 0 & 0 & 0 \\ a_3 & a_2 & 0 & 0 \\ 0 & a_4 & a_2 & 0 \\ 0 & 0 & a_5 & a_2 \end{bmatrix} \begin{bmatrix} P_1 \\ P_2 \\ P_3 \\ P_4 \end{bmatrix} \quad (65)$$

subject to the boundary conditions  $P_1(L, t) = Q$ ,  $P_{i \neq 1}(L, t) = 0$ .

Similarly, we assume a solution for the linearized Euler equation of the form

$$\Delta p_0(x, t) = S_1(x, t) \Delta p_0(L, t) + S_2(x, t) \Delta v(t) + S_3(x, t) \Delta \dot{m}_{in}(t) + S_4(x, t) \Delta T_{0,in}(t) \quad (66)$$

Substituting this into Eq. (58) and again neglecting the term  $\Delta p_{0,t}$ , we obtain a quasi-steady state equation as

$$\frac{\partial}{\partial x} \begin{bmatrix} S_1 \\ S_2 \\ S_3 \\ S_4 \end{bmatrix} = - \begin{bmatrix} a_2 & 0 & 0 & 0 \\ 0 & a_2 & 0 & 0 \\ 0 & 0 & a_2 & 0 \\ 0 & 0 & 0 & a_2 \end{bmatrix} \begin{bmatrix} S_1 \\ S_2 \\ S_3 \\ S_4 \end{bmatrix} - \begin{bmatrix} 0 \\ a_3 \\ a_4 \\ a_5 \end{bmatrix} \quad (67)$$

with the boundary conditions  $S_1(L, t) = 1$ , and  $S_{i \neq 1}(L, t) = 0$ .

Applying the boundary condition (59) and solving for  $\Delta v$  then yields

$$\Delta v(t) = \frac{1}{S_2(0, t)} [\Delta p_0(0, t) - S_1(0, t) \Delta p_0(L, t) - S_3(0, t) \Delta \dot{m}_{in}(t) - S_4(0, t) \Delta T_{0,in}(t)] \quad (68)$$

Substituting Eq. (68) back into Eq. (66) results in

$$\begin{aligned} \Delta p_0(x, t) = & \left[ S_1(x, t) - S_1(0, t) \frac{S_2(x, t)}{S_2(0, t)} \right] \Delta p_0(L, t) + \frac{S_2(x, t)}{S_2(0, t)} \Delta p_{0,in}(t) \\ & + \left[ S_3(x, t) - S_3(0, t) \frac{S_2(x, t)}{S_2(0, t)} \right] \Delta \dot{m}_{in}(t) + \left[ S_4(x, t) - S_4(0, t) \frac{S_2(x, t)}{S_2(0, t)} \right] \Delta T_{0,in}(t) \end{aligned} \quad (69)$$

Upon substituting Eqs. (69) and (64) into the optimal control expression in Eq. (63), we finally obtain a feedback form for the air injection mass flow control as

$$\Delta v(t) = K_1(t) \Delta p_0(L, t) + K_2(t) \Delta p_{0,in}(t) + K_3(t) \Delta \dot{m}_{in}(t) + K_4(t) \Delta T_{0,in}(t) \quad (70)$$

where  $K_i$ ,  $i = 1, \dots, 4$  are the optimal control gains defined as

$$\begin{aligned} K_1(t) &= \frac{\int_0^L a_3(x, t) P_1(x, t) \left[ S_1(x, t) - S_1(0, t) \frac{S_2(x, t)}{S_2(0, t)} \right] dx}{R - \int_0^L a_3(x, t) P_2(x, t) dx} \\ K_2(t) &= \frac{\int_0^L a_3(x, t) P_1(x, t) \frac{S_2(x, t)}{S_2(0, t)} dx}{R - \int_0^L a_3(x, t) P_2(x, t) dx} \\ K_3(t) &= \frac{\int_0^L a_3(x, t) \left\{ P_1(x, t) \left[ S_3(x, t) - S_3(0, t) \frac{S_2(x, t)}{S_2(0, t)} \right] + P_3(x, t) \right\} dx}{R - \int_0^L a_3(x, t) P_2(x, t) dx} \\ K_4(t) &= \frac{\int_0^L a_3(x, t) \left\{ P_1(x, t) \left[ S_4(x, t) - S_4(0, t) \frac{S_2(x, t)}{S_2(0, t)} \right] + P_4(x, t) \right\} dx}{R - \int_0^L a_3(x, t) P_2(x, t) dx} \end{aligned}$$

To ensure a non-singular optimal control, we must limit the value of the control weighting factor  $R$  such that

$$R \neq \int_0^L a_3(x, t) P_2(x, t) dx \quad (71)$$

From Eq. (70), it can be seen that the error-correction feedback control only depends on the total pressure error at the outlet  $\Delta p_0(L, t)$  as well as the disturbance inputs due to changes in the inlet condition of the stator cascade. The quasi-steady state control essentially transforms a control that depends on a total pressure error distribution along the stator cascade into one that only depends on the flow quantities at the stator inlet and outlet. Thus, it is a simpler type of feedback flow control as compared to a standard full-state feedback control scheme that would require the linearized Euler equation to be discretized and casted in a standard state space form. A standard LQR optimal control method<sup>18</sup> could then be implemented but would require the total pressure error distribution along the stator flow passage to be measured or estimated. Such a method is inherently more complex than the present quasi-steady state feedback control approach. Fig. 8 illustrates a block diagram of the quasi-steady state error-correction feedback optimal control.

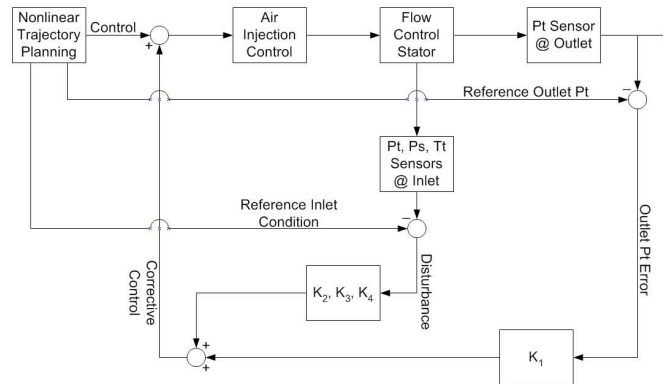


Fig. 8 - Quasi-Steady State Feedback Control Block Diagram

## IX. Results and Discussion

To demonstrate the flow control concept, a flow control simulation is performed. A representative mid-radius stator cascade is selected for the study. The notional stator blade has a NACA 65-series low speed profile, a camber angle of  $30^\circ$ , a stagger angle of  $45^\circ$ , and a solidity of 1, which is comparable to the LSAC flow control vane. The inlet condition is specified to be at a mass flow of 0.0222 slug/sec, a total pressure of 2116.2 psf, and a total temperature of 529.67 °R. Based on the resulting flow passage, an area distribution per unit length of the 2-D cascade duct along the mid-streamline is computed as shown in Fig. 9.

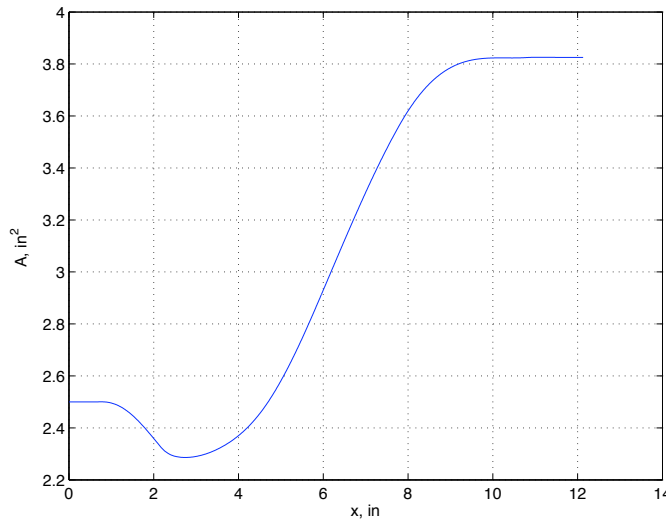


Fig. 9 - Area Distribution of Cascade Flow Passage

Fig. 9 reveals that the flow passage area decreases near the leading edge, thus indicating an accelerating flow as expected. The flow passage then opens up, forming a diffuser and thereby causing the flow to decelerate that

consequently results in a static pressure recovery from the kinetic energy of the flow. It is the adverse pressure gradient in a diffusing flow passage that tends to promote flow separation.

In order to model the stator cascade based on the 1-D unsteady Euler equations, the 2-D cascade duct is discretized into a finite number of computing stations that capture reasonably well the cascade geometry. A time step of 0.02 ms is selected so as to satisfy the Courant-Friedrichs-Levy (CFL) stability condition,<sup>17</sup> assuming that the flow remains subsonic throughout the flow passage. Applying the Nyquist frequency criterion, the frequency range of interest would be 25 kHz, which is adequate to address the frequency requirement of 10 kHz for actuation. Thus, using the time-accurate 1-D unsteady flow equations for flow control modeling would ensure that the high frequency requirement could be met.

An arbitrary inlet air angle of 60° is selected. This air inlet angle results in an angle of attack of 15°. The performance of this cascade is then predicted by a NACA 65-series cascade correlation method based on the Carter's rule

$$\Delta\beta = \beta_1 - \beta_2 = i_0 - \delta_0^0 + \theta(1 - m + n) \quad (72)$$

where  $\Delta\beta$  is the turning angle,  $i_0$  is the reference minimum-loss incidence angle,  $\delta_0^0$  is the reference deviation angle at the reference incidence angle,  $\theta$  is the blade camber angle, and  $m$  and  $n$  are the slope parameters as functions of the air inlet angle  $\beta_1$  and the solidity  $\sigma$ .<sup>8</sup>

The Carter's rule predicts an outlet air angle of 40° or a 20° turning angle. The difference of 10° from the blade camber angle is the flow deviation angle which is due to flow separation that normally occurs on the suction surface. The diffusion factor for this cascade as computed from Eq. (3) is 0.6078 which exceeds a recommended maximum diffusion factor of 0.55 for stall free operation and corresponds to a total pressure loss coefficient of 0.1910. To reduce the tendency for flow separation, we would like to reduce the diffusion factor to about 0.5, which correspond to a total pressure loss coefficient of 0.1228. So, we would like to seek a total pressure set point of 2060.1 psf or an air injection mass flow of  $1.1104 \times 10^{-4}$  slug/sec which is about 0.5% of the total mass flow. The optimal control trajectory is computed from the nonlinear trajectory optimization using the second-order gradient method with weighting factors  $Q = 1 \times 10^{-5}$  and  $R = 1 \times 10^8$  for the cost function. The computation converges rapidly to the optimal solution within two iterations. The air injection mass flow time history as shown in Fig. 10(a) exhibits an initial oscillation before quickly settling to the desired air injection mass flow. Fig. 10(b) shows the total pressure response at the outlet lagging the air injection mass flow control by a small time delay as a result of the fluid transport process.

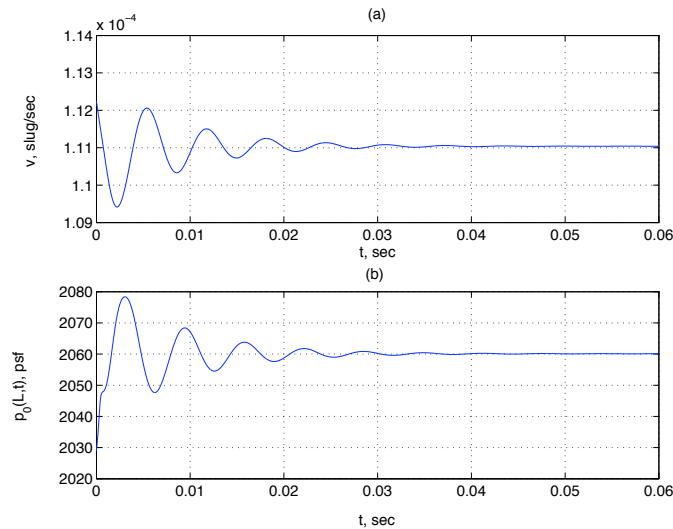


Fig. 10 - (a) Nonlinear Optimal Air Injection Control and (b) Total Pressure Response at Outlet

Fig. 11 illustrates an optimal trajectory of the gain schedule as a function of the total pressure error from the set point at the outlet. The gain schedule allows the air injection mass flow control to be computed as follows

$$v(t) = v_d + K_{opt} [p_0(L, t) - p_{0,d}(L)] + K_{opt} p_{0,d}(L) \quad (73)$$

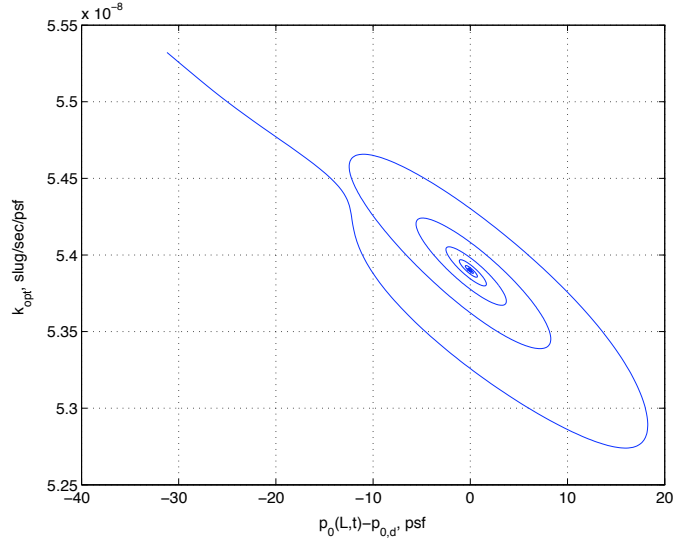


Fig. 11 - Gain Schedule

Fig. 12(a) shows the total pressure distribution along the cascade flow passage with the air injection control on and off. It is noted that near the leading edge, the flow is modeled as loss-free because of the convergent flow passage wherein the boundary layer is thinned resulting from a favorable pressure gradient associated with an accelerating flow as seen in Fig. 12(b). At the point of maximum velocity, the total pressure rapidly decreases due to the boundary layer thickening in the divergent flow passage. With the air injection control on, the total pressure at the outlet is raised above that with no air injection control, thus effectively reducing the total pressure loss. The total pressure distribution as computed by the Euler equations is also plotted as a surface function of space and time in Fig. 13. The velocity distributions as shown in Fig. 12(b) are similar with and without air injection control. The outlet velocity with no air injection control is slightly higher than that with the air injection control as expected. Without the air injection control, the outlet tangential velocity component should be higher, corresponding to a lower air turning angle, than it would be if the air injection control is on.

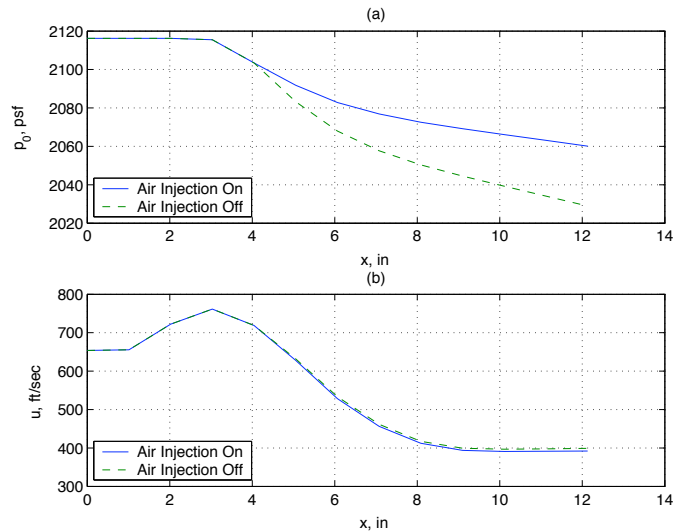


Fig. 12 - (a) Total Pressure Distribution and (b) Velocity Distribution

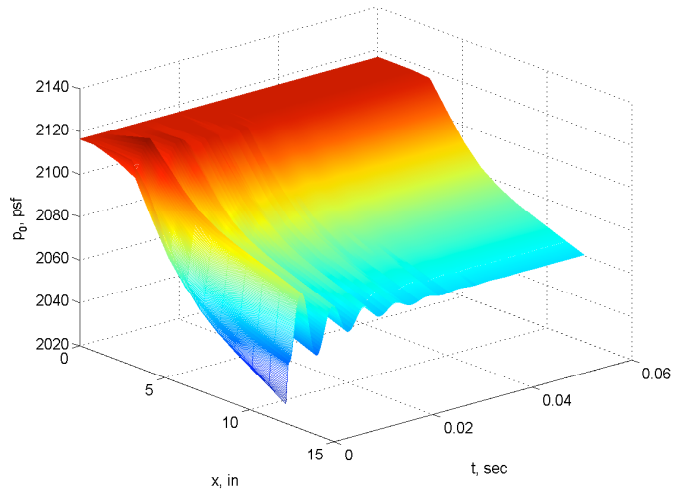


Fig. 13 - Total Pressure Response Surface

To demonstrate the error-correction feedback control, we synthesize a variation in the inlet flow condition that results in a mass flow perturbation of  $1.2163 \times 10^{-4}$  slug/sec, a total pressure perturbation of 10.6 psf, and a total temperature perturbation of 2.68 °R. The error-correction feedback control is computed using the quasi-steady state method with weighting factors  $Q = 1 \times 10^{-2}$  and  $R = 1$ . The optimal quasi-steady state feedback gains are plotted in Fig. 14. The optimal feedback corrective air injection mass flow control is plotted in Fig. 15(a) and the resulting total pressure error response is plotted in Fig. 15(b). We note that the total pressure error does not quite reach zero as the control incurs a very small steady state error. This steady state error is due to the lack of an integral feedback in the control. Nonetheless, the quasi-steady state feedback control is quite effective in controlling the total pressure at the outlet.

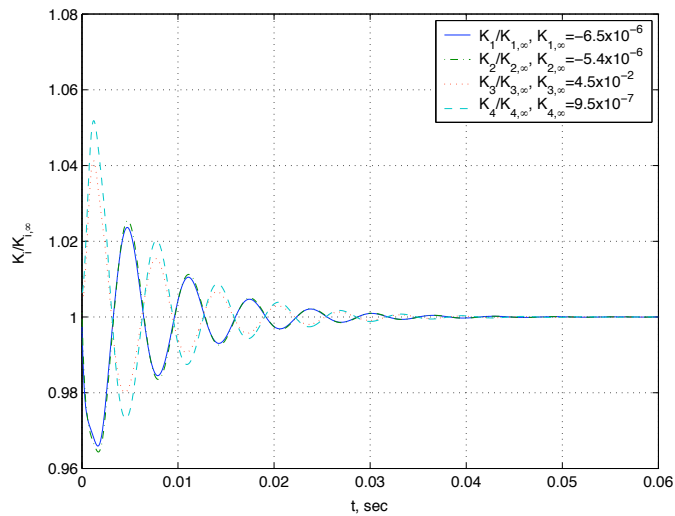


Fig. 14 - Quasi-Steady State Feedback Gain Ratios

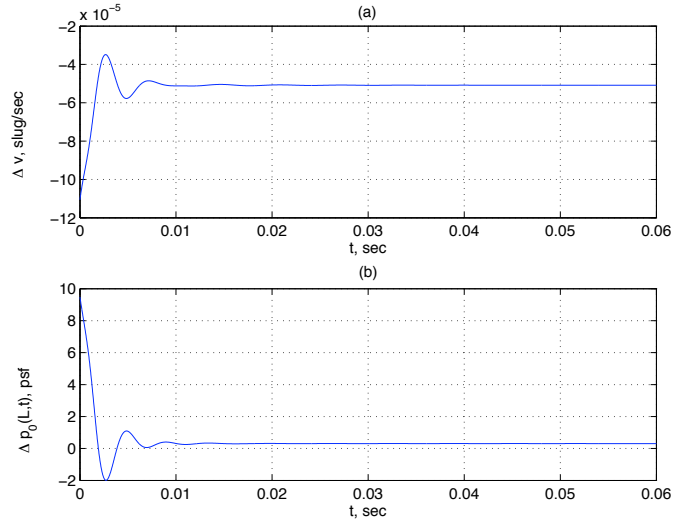


Fig. 15 - (a) Quasi-Steady State Corrective Air Injection Mass Flow Control and (b) Total Pressure Error Response at Outlet

It should be noted that in the present flow control method, we have not considered the effects of dynamics of the air injection mass flow control valve and line loss in the pressure tubing. In practice, these effects can potentially limit the overall performance of the flow control design. Typically, flow control valves tend to have longer time constants than the fluid transport time. As a result, the actual response of the air injection mass flow is likely slower than the computed trajectory. However, the steady state value of the air injection mass flow should still be achievable if the flow control valve has a sufficient range. Thus, to improve the frequency response of the flow control, a flow control valve with a desirable frequency performance should be selected. The effect of line loss in the pressure tubing is generally more adverse than the dynamics of the flow control valve. If the pressure tubing from the bleed air reservoir is significantly long, the mass flow will likely be throttled down due to the line loss effect. This would potentially result in an under-actuated control whereby the flow control valve would not be able to deliver the correct air injection mass flow. Moreover, the line loss effect also causes a time delay in the delivery of the air injection mass flow. Therefore, it is important that the pressure tubing be kept as short as possible in order to maintain a proper performance of the flow control.

The issue of sensor placements is critical in designing an effective flow control. Real flow in a compressor cascade exhibits a tangential variation. Since the pressure loss parameter is determined from the tangentially average total pressure quantities, the cascade flow passage at the inlet and outlet should be covered sufficiently with total pressure sensors. Alternatively, a single sensor could be placed at a strategic location that allows it to measure a local total pressure quantity that is approximately equal to the tangentially average total pressure quantity. Fig. 16 shows a sample of three tangential variations of the total pressure measurements normalized to the flow-weighted tangentially average total pressure at the stator inlet and outlet in the LSAC test facility. The abscissa  $n\theta/2\pi$  is the tangential coordinate of the flow passage around one stator blade with  $0 \leq n\theta/2\pi < 1/2$  being the flow region below the pressure surface. As can be seen, the total pressure at the outlet exhibits a sharp wake at the trailing edge. Based on these total pressure profiles, it appears that a single total pressure sensor could be placed at  $n\theta/2\pi \approx 0.32$  at the inlet and the outlet where the local total pressure is about equal to the average total pressure. The advantage of a single sensor location is the simplicity in the sensor design that would eliminate the needs for computing the tangentially average total pressure. This in turn would reduce the computational overhead in the feedback flow control implementation.

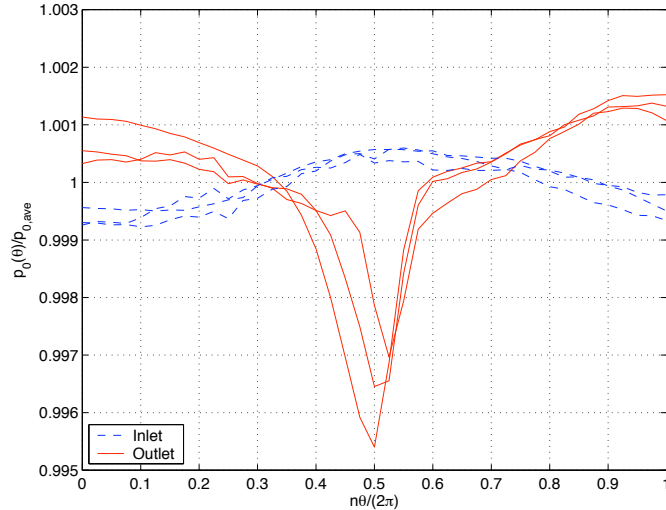


Fig. 16 - Tangential Variations of Total Pressure at Stator Inlet and Outlet

## X. Conclusion

This paper has presented a flow control method using air injection as a means for flow separation control in a compressor stator cascade. The flow control is based on a fluid-physics model using the 1-D unsteady Euler equations with a total pressure loss parameter that represents the viscous dissipation associated with flow separation in a compressor cascade. The air injection mass flow control is posed as an interior pointwise control within the stator flow passage. The total pressure loss parameter is estimated using a recursive least-square parameter estimation process based on a quadratic relationship that describes the effect of the air injection mass flow control on the total pressure loss reduction. A nonlinear control trajectory optimization is derived from a continuous adjoint method that establishes the necessary conditions for optimality of the 1-D Euler equations with an interior pointwise control. A computational procedure for implementing a second-order gradient method is presented to describe a solution method for solving a two-point boundary value problem involving the Euler and adjoint equations. The optimization method is implemented numerically and demonstrates a rapid convergence due to the quadratic relationship of the air injection mass flow control. A quasi-steady state error-correction feedback method for a linearized momentum equation has been introduced. A simulation shows that this new feedback flow control method is very effective in controlling the total pressure error at the stator outlet due to flow disturbances at the stator inlet.

## References

- <sup>1</sup>Lord, W. K., MacMartin, D. G., and Tillman, T. G., "Flow Control Opportunities in Gas Turbine Engines", *AIAA Fluids Conference*, AIAA-2000-2234, June 2000.
- <sup>2</sup>MacMartin, D. G., Murray, R. M., Verma, A., and Paduano, J. D., "Active Control of Integrated Inlet/Compression Systems: Initial Results", *2001 ASME Fluids Engineering Division Summer Meeting*, FEDSM2001-18275, June 2001.
- <sup>3</sup>Leinhos, D. C., Scheidler, S. G., and Fottner, L., "Experiments in Active Stall Control of a Twin-Spool Turbofan Engine", *Proceedings of ASME TURBO EXPO 2002*, GT-2002-30002, June 2002.
- <sup>4</sup>d'Andrea, R., Behnken, R. L., and Murray, R. M., "Active Control of an Axial Flow Compressor via Pulsed Air Injection", *California Institute of Technology CDS Report 95-029*, July 1996.
- <sup>5</sup>Culley, D. E., Bright, M. M., Prahst, P. S., and Strazisar, A. J., "Active Flow Separation Control of a Stator Vane Using Surface Injection in a Multistage Compressor Experiment", *Proceedings of ASME TURBO EXPO 2003*, GT2003-38863, June 2003.
- <sup>6</sup>Moore, F. K., and Greitzer, E. M., "A Theory of Post-Stall Transients in Axial Compression Systems: Part I Development of Equations", *Journal of Engineering for Gas Turbines and Power*, Vol. 108, Jan 1986.
- <sup>7</sup>Blevins, R. D., *Applied Fluid Dynamics Handbook*, Van Nostrand Company, New York, 1984.
- <sup>8</sup>National Aeronautics and Space Administration, *Aerodynamic Design of Axial-Flow Compressors*, NASA SP-36, 1965.
- <sup>9</sup>Dixon, S. L., *Fluid Mechanics - Thermodynamics of Turbomachinery*, 3rd Edition, Pergamon Press, New York, 1989.
- <sup>10</sup>Ravindran, S. S., "Reduced-Order Adaptive Controllers for Fluid Flows Using POD", *Journal of Scientific Computing*, 2000; 15(4): 457-478.
- <sup>11</sup>Shapiro, A. H., *The Dynamics and Thermodynamics of Compressible Fluid Flow*, Volume II, Ronald Press Company, New York, 1954.
- <sup>12</sup>Stengel, R. F., *Optimal Control and Estimation*, Dover Publications, Inc., New York, 1994.

<sup>13</sup>Becker, R., Kapp, H., and Rannacher, R., "Adaptive Finite Element Methods for Optimal Control of Partial Differential Equations: Basic Concept", *SIAM Journal on Control and Optimization*, Vol. 39, No. 1, 2000, pp. 113-132.

<sup>14</sup>Jameson, A., Pierce, N., Martinelli, L., "Optimum Aerodynamic Design Using the Navier-Stokes Equations", *Theoretical Computational Fluid Dynamics*, Vol. 10, 1998, pp. 213-237.

<sup>15</sup>Nadarajah, S., and Jameson, A., "A Comparison of The Continuous and Discrete Adjoint Approach to Automatic Aerodynamic Optimization", *AIAA Conference*, AIAA-2000-0667, January 2000.

<sup>16</sup>Nguyen, N., and Ardema, M., "Optimal Control of Flow Recirculation in a Wind Tunnel", *AIAA Guidance, Navigation, and Control Conference*, AIAA-2004-4759, August 2004.

<sup>17</sup>Hirsh, C., *Numerical Computation of Internal and External Flows*, Vol. 1, John Wiley & Sons, Brussels, 1991.

<sup>18</sup>Brogan, W. L., *Modern Control Theory*, 3rd Edition, Prentice Hall, New Jersey, 1991.